PROCEEDINGS of the
23rd International Congress on Acoustics

9 to 13 September 2019 in Aachen, Germany

Numerical investigation of indirect combustion noise mechanisms in a nozzle

Thomas DECONINCK[1]; Antoine VALLON[2]; Alexis APPEL DE GARDANE[1] ; Yves DETANDT[1] ; César LEGENDRE[1] and Grégory LIELENS[1]

[1] Free Field Technologies, MSC Software Belgium

[2] Safran Helicopter Engines

ABSTRACT

The entropy and vorticity disturbances generated in the combustion chamber of an aero-engine can be converted into pressure fluctuations while accelerated in the turbine stages: this phenomenon is known as Indirect Noise. The mean flow plays a significant role in this process and should be considered in the modeling. As a first step, the present paper focus on modeling the interaction of entropy and acoustic waves in a nozzle. First, the mean flow inside the nozzle is estimated by means of a steady-state CFD simulation. Second, the wave propagation including the mean flow effects is computed by means of a high-order adaptive Discontinuous Galerkin (DG) scheme in time domain solving the linearized Euler equations (LEE). This scheme is chosen due to its ability to accurately represent the phenomena involved and its high parallel scalability. The studied cases consist of a convergent/divergent nozzle configuration where entropy waves are injected upstream by means of strong heat pulses. Three representative flow conditions with different mass flow rates are considered. Finally, the numerical solutions are compared with available experimental data and analytical models showing good agreement.

Keywords: Sound, Combustion Noise, Indirect Noise

1. INTRODUCTION

Combustion noise in aero-engines can be decomposed into direct combustion noise and indirect combustion noise. The strong unsteadiness of the combustion chamber itself is responsible for the direct combustion noise, whose acoustic waves traverse the turbine stages. Indirect combustion noise is caused by the generation of acoustic waves within the turbine stages when temperature inhomogeneities (associated with entropy spots) are accelerated through those stages.

Assuming a quasi-one-dimensional nozzle, Marble & Candle [1] derived wave transfer functions linking entropy and acoustic waves for both subsonic and chocked nozzles. Their model has been well demonstrated for compact cases, i.e. when one considers the axial length of the nozzle to be small compared to the wavelength of the acoustic or entropy perturbations limiting the results to low frequencies. In the same manner, the Cumpsty & Marble model [2] applies the actuator disk theory to mimic the acoustic behavior of turbine stages taking into account also the azimuthal modes, as well as the mean flow deviation with respect to the axis. These two above mentioned models constitute a computationally inexpensive modeling technique to assess the indirect combustion noise in a nozzle using the compact assumption.

Full numerical simulations of the Linearized Euler Equations (LEE) offer an alternative to model the combustion noise through the turbine stages. The LEE allow evaluating the propagation of any kind of small perturbations (acoustic or not) within a given mean flow assuming isentropic and inviscid conditions. Actran DGM (from the commercial software FFT) solves the LEE in the time domain using a quadrature-free Runge-Kutta discontinuous Galerkin method (RK-DGM) [3]. It is implemented for unstructured grids in 2D, 2D axisymmetric and 3D and employs a fourth order Runge-Kutta temporal scheme and supports variable order of the elements (p-adaptivity).

In the present work, we aim at assessing the mentioned modeling techniques for indirect noise

through the experimental Entropy Wave Generator (EWG) from the DLR [4,5], which has been simulated by many groups. Section 2 describes the modeling technique approaches, with one subsection dedicated to the Marble & Candel model with the compact assumption and the second subsection dedicated to the LEE model in Actran DGM. A description of the EWG experimental setup is presented in section 3. Numerical and experimental data are analyzed in section 4 and conclusions are finally discussed in section 5.

2. INDIRECT COMBUSTION NOISE

2.1 The compact model

As wavelengths of the disturbances considered here are much larger than the axial length of the nozzle, acoustic and entropy waves propagate quasi-steadily through the flow. Based on first principles conservation laws (for the mass flow rate, the total temperature and the entropy), matching conditions are imposed between the region upstream of the nozzle and the region downstream of the nozzle. Marble & Candel [1] derived expressions for the up- and downstream propagating acoustic pressure perturbations (traveling from the inlet to the outlet or conversely and indicated by the superscripts "+" and "-", respectively) generated by both impinging entropy disturbances and impinging acoustic pressure waves. The responses to acoustic wave and entropy disturbances when considering a subsonic flow, are presented in Table 1.

Acoustic wave upstream ($P_1^+ = \varepsilon$)	*Acoustic wave downstream* ($P_2^- = \varepsilon$)
$P_1^+ = \varepsilon,\ P_2^- = 0$	$P_1^+ = 0,\ P_2^- = \varepsilon$
$P_1^- = \left(\frac{M_2 - M_1}{1 - M_1}\right)\left(\frac{1 + M_1}{M_2 + M_1}\right)\left[\frac{1 - \frac{1}{2}(\gamma - 1)M_1M_2}{1 + \frac{1}{2}(\gamma - 1)M_1M_2}\right]\varepsilon$	$P_1^- = \left(\frac{2M_1}{M_1 + M_2}\right)\left(\frac{1 - M_2}{1 - M_1}\right)\left[\frac{1 + \frac{1}{2}(\gamma - 1)M_1^2}{1 + \frac{1}{2}(\gamma - 1)M_1M_2}\right]\varepsilon$
$P_2^+ = \left(\frac{2M_2}{1 + M_2}\right)\left(\frac{1 + M_1}{M_2 + M_1}\right)\left[\frac{1 + \frac{1}{2}(\gamma - 1)M_2^2}{1 + \frac{1}{2}(\gamma - 1)M_1M_2}\right]\ \varepsilon$	$P_2^+ = -\left(\frac{M_2 - M_1}{1 + M_2}\right)\left(\frac{1 - M_2}{M_2 + M_1}\right)\left[\frac{1 - \frac{1}{2}(\gamma - 1)M_1M_2}{1 + \frac{1}{2}(\gamma - 1)M_1M_2}\right]\varepsilon$
Convected entropy wave ($s'/c_p = \sigma$)	
$P_1^+ = 0,\ P_2^- = 0$	
$P_1^- = -\left(\frac{M_2 - M_1}{1 - M_1}\right)\frac{\frac{1}{2}M_1\sigma}{1 + \frac{1}{2}(\gamma - 1)M_1M_2}$	
$P_2^+ = \left(\frac{M_2 - M_1}{1 + M_2}\right)\frac{\frac{1}{2}M_2\sigma}{1 + \frac{1}{2}(\gamma - 1)M_1M_2}$	

Table 1. Compact acoustic and entropy transfer functions in a subsonic nozzle

The acoustic processes in a choked nozzle differ since the acoustic waves in the supersonic divergent cannot propagate to the convergent. For such supercritical nozzle, Marble & Candel [1] derived expressions of the transfer functions as shown in Table 2. A configuration in which a normal shock is located downstream of the nozzle, as illustrated in Figure 1, had also been considered in their original model.

Acoustic wave upstream ($P_1^+ = \varepsilon$)
$P_1^+ = \varepsilon, \qquad P_2^- = \frac{1 - \frac{1}{2}(\gamma - 1)M_2}{1 + \frac{1}{2}(\gamma - 1)M_1}\varepsilon$
$P_1^- = \frac{1 - \frac{1}{2}(\gamma - 1)M_1}{1 + \frac{1}{2}(\gamma - 1)M_1}\varepsilon$

$P_2^+ = \dfrac{1+\frac{1}{2}(\gamma-1)M_2}{1+\frac{1}{2}(\gamma-1)M_1} \quad \varepsilon$	
Convected entropy wave $(s'/c_p = \sigma)$	*Convected entropy wave with shock* $(s'/c_p = \sigma)$
$P_1^+ = 0, \qquad P_2^- = -\left(\dfrac{M_2+M_1}{2}\right)\dfrac{\frac{1}{2}\sigma}{1+\frac{1}{2}(\gamma-1)M_1}$	$P_1^+ = 0$
$P_1^- = -\dfrac{\frac{1}{2}M_1\sigma}{1+\frac{1}{2}(\gamma-1)M_1}$	$P_1^- = -\dfrac{\frac{1}{2}M_1\sigma}{1+\frac{1}{2}(\gamma-1)M_1}$
$P_2^+ = \left(\dfrac{M_2-M_1}{2}\right)\dfrac{\frac{1}{2}\sigma}{1+\frac{1}{2}(\gamma-1)M_1}$	$P_3^+ = \left[\dfrac{-(1+M_2^2)M_1+2M_2^2M_3^2}{1+M_2^2+2M_2^2M_3}\right]\dfrac{\frac{1}{2}\sigma}{1+\frac{1}{2}(\gamma-1)M_1}$

Table 2. Compact acoustic and entropy transfer functions in a choked nozzle

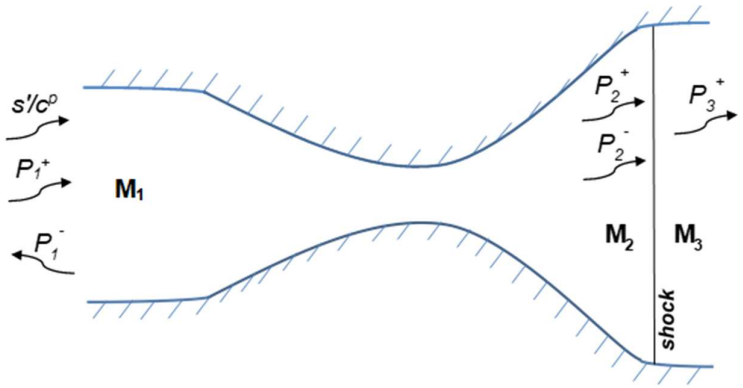

Figure 1. Supersonic nozzle with a normal shock downstream

2.2 The LEE model in Actran DGM

Actran DGM solves the LEE in the time domain by means of a Discontinuous Galerkin Methods. As the LEE are derived from the compressible Navier-Stokes equations, the LEE isentropic set of equations is made of five partial differential equations. The isentropic equations propagate not only the acoustic fluctuations (the upstream propagating acoustic mode characterized by the propagation speed v^0-c and the downstream propagating acoustic mode characterized by the propagating speed v^0+c), but also two vortical modes and one entropy mode (characterized by the propagating speed v^0). The system of equations supports the acoustic propagation in supersonic mean flows and can be solved for the acoustic propagation through a shock.

The element boundary integrals in the DGM scheme are computed by considering the solution in the two adjacent elements. The scheme is designed to enforce a stable solution during the propagation of waves from one element to the other. For free field propagation, a non-reflecting boundary enforces that all the incoming modes are set to zero, the outgoing modes being free to leave the domain. At the inlet, a Thompson condition has been introduced to avoid this reflective character of the traditional boundary conditions. For our case of interest, the incoming entropy wave is simulated with an applied density perturbation at the boundary, while the pressure and velocity fluctuations are set to zero.

3. Experimental configuration

The Entropy Wave Generator (EWG) is a nozzle with the capability of inducing entropy waves via a heating module [5]. The experimental setup is shown in Figure 2 while the nozzle itself is sketched in Figure 3. In order to create an entropy wave, a temperature pulse is generated through a heat generator. The temperature pulse is a step with a duration of 100 ms, which occurs every second.

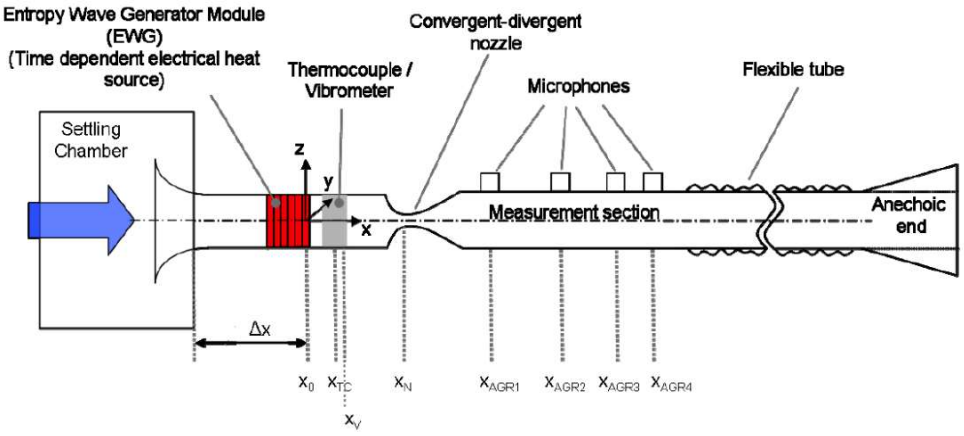

Figure 2. Sketch of the Entropy Wave Generator (EWG)

Figure 3. Sketch of the convergent-divergent nozzle

Three representative flow conditions with different mass flow rates are considered. The flow is either supersonic (EWG1), subsonic (EWG2), or almost supersonic (EWG3). These flow conditions had already been used for the European project RECORD [6] and are summarized in Table 3. All data come from measurements except for the Mach numbers upstream and downstream of the nozzle and the Mach number before shock that come a 1D flow code (which had been developed in the framework of the RECORD project).

Test case	Mass flow rate [kg/h]	Pressure setting chamber against ambient pressure [kPa]	Pressure nozzle throat against ambient pressure [kPa]	Mach number upstream the nozzle	Mach number downstream the nozzle	Mach number at nozzle throat	Mach number before shock
EWG 1	42	11.17	-52.71	0.029	0.023	1.0	1.59
EWG 2	37	4.34	-32.65	0.027	0.019	0.71	-
EWG 3	40	7.34	-45.49	0.028	0.020	0.87	-

Table 3. Experimental flow conditions of the EWG

4. Aeroacoustic simulations

4.1 Numerical model

In Actran DGM, Euler's equations are linearized around a stationary mean flow. Therefore, in order to steer the LEE model, a simulation of the nozzle has been performed with the CFD software OpenFOAM. The boundary layer is not modelled (wall slip boundary conditions at the nozzle walls) and the density-based version of the solver has been considered without any turbulence model. An axi-symmetric mesh with 32 000 cells has been built with the ANSA software. Details regarding the boundary conditions for the supersonic case (EWG1) are shown in Figure 4.

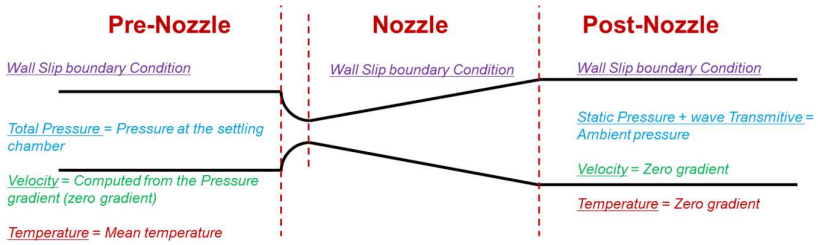

Figure 4. CFD boundary conditions

As shown in Figure 5, the Actran DGM model uses a similar domain as the CFD domain, but evidently with different types of boundary conditions. The excitation is injected in the model through a Thompson boundary condition, while the semi-infinite duct is modelled with a buffer zone and a non-reflecting boundary condition. An acoustic mesh has been built for the LEE model, comprising about 9000 elements, capturing not only the acoustics at 200 Hz, but also the geometrical features of the nozzle.

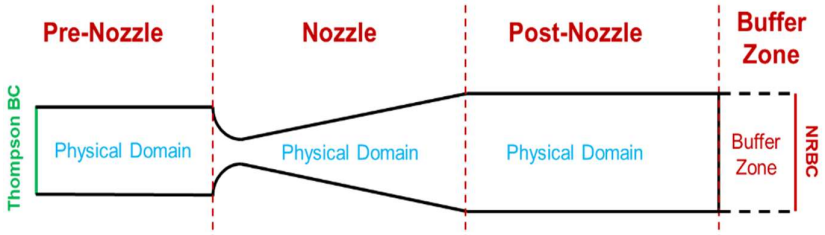

Figure 5. Components and boundary conditions of the Actran DGM model

For the simulations performed with the compact model, the nozzle domain is simply bypassed through a transfer admittance and with non-reflecting boundary conditions at the inlet and outlet. At the inlet, the entropy signal is evaluated with the expression given in equation (1), while the density signal is evaluated with the expression given in equation (2) in the Thompson boundary condition of Actran DGM.

$$s' = \frac{Cp}{T0} * T' \tag{1}$$

$$\rho'_{exp} = -\frac{\rho 0}{Cp} * s' = -\frac{\rho 0}{T0} * T' \tag{2}$$

Looking at Figure 6, one can see that the experimental temperature signal includes notable noise. Instead, an equivalent analytical signal has been considered in this study, whose expressions are given in equations (3)-(4)-(5). The numerical values of t_{min}, t_{max}, τ_{min}, and τ_{max} have been obtained by a least square fit from the original experimental signal. The differences between the experimental and analytical signal are the strongest at high frequencies, as shown in Figure 6.

$$T(t) = 0 \quad if \quad t < t_{min} \tag{3}$$

$$T(t) = A \cdot \left(1 - e^{\frac{t - t_{min}}{\tau_{min}}}\right) \quad if \quad t_{min} < t < t_{max} \tag{4}$$

$$T(t) = A \cdot \left(e^{\frac{t - t_{max}}{\tau_{max}}}\right) \quad if \quad t_{max} < t \tag{5}$$

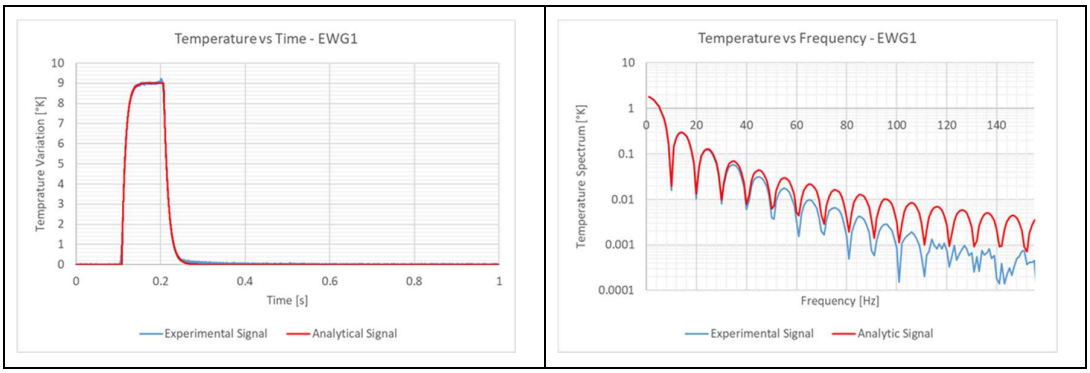

Figure 6. Experimental vs analytical temperature signal in the time (left) and frequency (right) domains

It has been observed that Kelvin-Helmholtz instabilities occur in the Actran DGM model at low frequencies and in the presence of high velocity gradients in the divergent section. These instabilities prevent the computation convergence, and so decrease the results accuracy. To avoid this, the flow variations in the radial direction have been removed to keep only the flow variations in the axial direction, as illustrated in Figure 7 for the test case EWG1. By considering an equivalent 1D flow (with a solver that had been developed in the framework of the RECORD project), the hydro-dynamic instabilities are strongly reduced and allows the computation to converge at very low frequencies. This simplification does not reduce the accuracy of the acoustic simulations with Actran DGM.

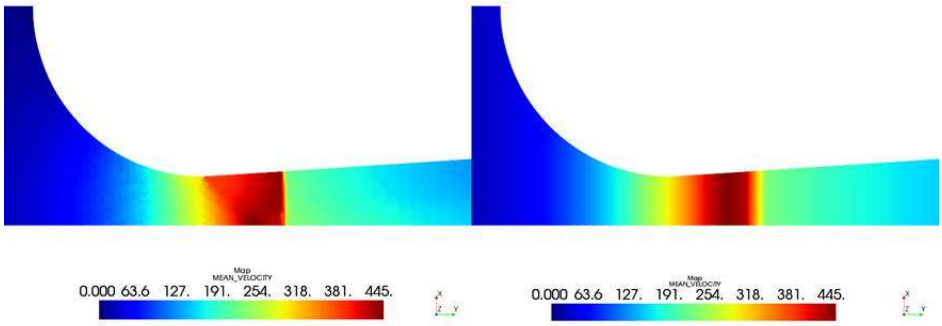

Figure 7.Original mean velocity flow from axi-symmetric model (left) vs equivalent 1D velocity flow (right)

4.2 Numerical results

In this section a comparison of the EWG data with numerical results obtained with the compact model and the LEE model is presented. For brevity purposes, we will show results only for microphone 1 and 4 (see Figure 2) even though, from the test case description with the anechoic boundary conditions, the results should not differ in between those microphones. We start considering the first test case, EWG1, in which a shock occurs in the downstream section of the nozzle. In the compact model, the Mach numbers upstream and downstream of the nozzle, as well as the Mach number before the shock are considered as inputs (see Table 3).

We observe differences in the experimental results at higher frequencies in between microphone 1 and 4 that may indicate some type of reflections at the exit. As shown in Figure 8, the comparison in between the compact and LEE model shows a very good match and, globally, there is also a good agreement with the experimental results.

For the EWG2 test case, the flow remains subsonic through the nozzle, with a maximum Mach number of 0.71 at the throat. For this test case and using the compact model of Marble and Candel [1], only the Mach values at the inlet and outlet of the nozzle should in principle be taken into account. Nevertheless, the model does barely transform entropy into acoustics when both Mach numbers values are comparable. As proposed by Bake *et al.* [4], the model has been distinctly split into an upstream nozzle and a downstream diffuser considering the Mach number at the throat as extra input. The impinging entropy disturbances enter the nozzle generating acoustic disturbances, and those acoustic disturbances are solely transmitted in the diffuser (as for the supersonic cases when acoustic

perturbations from the diffuser cannot propagate back to the nozzle). Some questions remain over the validity of this model and other authors have proposed alternatives (see Duran & Moreau [7] for example).

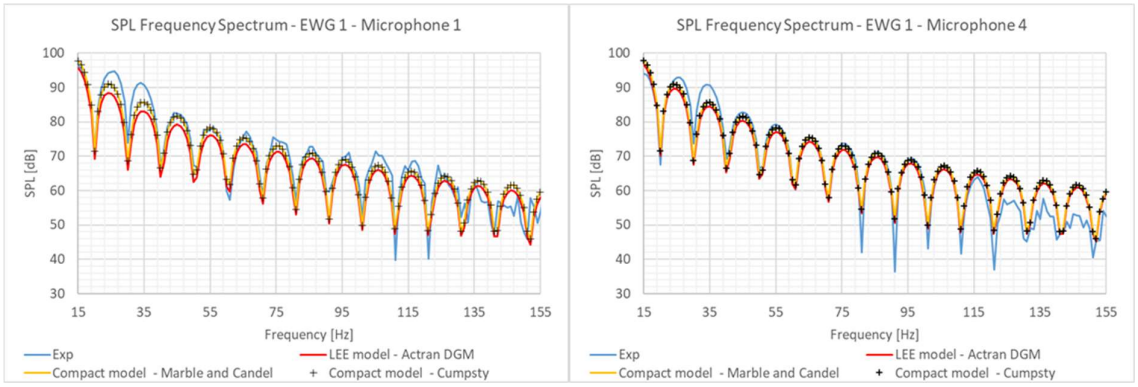

Figure 8. Acoustic pressure spectrum at microphones 1 and 4 (EWG1)

The DGM method had convergence issues for microphone 1 at low frequencies, therefore the results below 45 Hz are not presented. Apart from this, the overall agreement in between the proposed models and the experimental results is quite good, as shown in Figure 9.

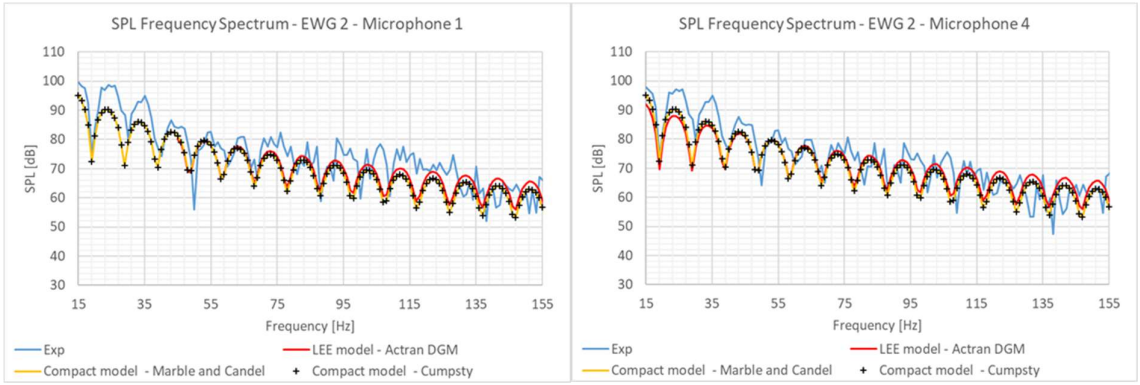

Figure 9. Acoustic pressure spectrum at microphones 1 and 4 (EWG2)

For the EWG3 test case, the flow becomes almost sonic at the throat (M = 0.88 on the axis). The same methodology as for the EWG2 test case has been applied in the numerical model. For this test case, the DGM method had convergence issues for microphone 1 at low frequencies, therefore the results below 65 Hz are not presented. As for the other test cases, the overall agreement in between the proposed models and the experimental results is quite good (see Figure 10).

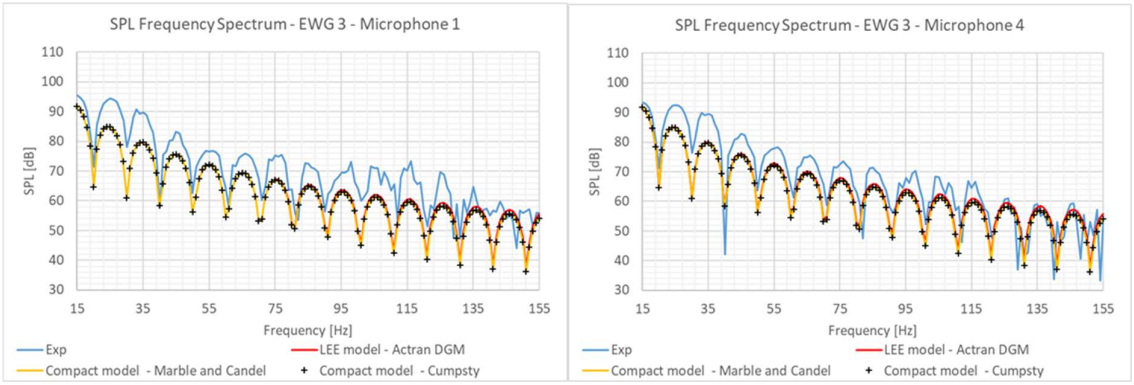

Figure 10. Acoustic pressure spectrum at microphones 1 and 4 (EWG3)

5. Conclusions

This study focused on the application of the compact model from Marble and Candel [1] and a LEE model from Actran DGM to the EWG test case, which is a convergent-divergent nozzle.

Three representative flow conditions have been considered and have been computed with OpenFOAM using an axi-symmetric model:

- EWG1: Supersonic flow at the nozzle throat followed by a shock in the diffuser
- EWG2: Subsonic flow at the nozzle throat
- EWG3: Almost sonic flow at the nozzle throat

Few assumptions have been made in the numerical set-up. A clean equivalent analytical signal has been considered as input for the entropy disturbances and the radial variations of the CFD results feeding the LEE model have been suppressed. Also, the Marble and Candel model has been adapted for subsonic cases with distinct treatment for the upstream nozzle and the diffuser. Comparison of the EWG data with numerical results have been presented and show a good agreement between the implemented models and the experimental data. As expected, the Cumpsty and Marble model [2] produces exactly the same results as the Marble and Candel model for this test case.

Future work will focus on the validation of the numerical models with realistic turbine cases (see for example [8],[9]). The LEE model from Actran DGM should turn out to be more accurate for those industrial test cases as less restrictions with respect to the compact model are applied.

ACKNOWLEDGEMENTS

Part of this work and the experimental results on EWG have been funded by the European Commission with the 7th Framework Program (Project RECORD grant 312444). The authors acknowledge their financial support.

REFERENCES

1. F.E. Marble and S. Candel, Acoustic disturbances from gas non-uniformities convected through a nozzle, J. Sound Vib. 55 (1977) 225–243.
2. N.A. Cumpsty and F.E. Marble, The interaction of entropy fluctuations with turbine blade rows; a mechanism of turbojet engine noise, Proc. R. Soc. Lond. A357 (1977) 323–344.
3. R. Leneveu, B. Schiltz, J. Manera, and S. Caro, Parallel DGM scheme for LEE applied to axhaust and bypass problems, 13th AIAA/CEAS Aeroacoustics Conference (2007), AIAA Paper 2007-3510.
4. F. Bake, U. Michel and I. Röhle, Experimental investigation of the fundamental entropy noise mechanism in aero-engines, 13th AIAA/CEAS Aeroacoustics Conference (2007), AIAA Paper 2007-3694.
5. F. Bake, C. Richter, B. Mühlbauer, N. Kings, I. Röhle, F. Thiele and B. Noll, The Entropy Wave Generator (EWG): A reference case on entropy noise, J. Sound Vib. 326 (2009) 574–598.
6. RECORD - Research on Core Noise Reduction, https://www.xnoise.eu/about-x-noise/projects/generation-2-projects/record/
7. I. Duran and S. Moreau, Solution of the quasi-one dimensional linearized Euler equations using flow invariants and the Magnus expansion, J. Fluid Mech. 723 (2013) 190-231.
8. T. Livebardon, S. Moreau, L. Gicquel, T. Poinsot and E. Bouty, Combining LES of combustion chamber and an actuator disk theory to predict combustion noise in a helicopter engine, Combust. Flame 165 (2016) 272-287.
9. M. Lemoult, A. Vallon, M. Roger, Exhaust noise from helicopter turboshaft engines, Proceedings of the 8th International Symposium on Experimental and Computational Aerothermodynamics of Internal Flows Lyon, July 2007.